Applied Energy 291 (2021) 116839

Contents lists available at ScienceDirect

Applied Energy

journal homepage: www.elsevier.com/locate/apenergy

Organic Rankine cycle integrated with hydrate-based desalination for a sustainable energy–water nexus system

Tianbiao He [a,*], Jibao Zhang [a], Ning Mao [a], Praveen Linga [b,*]

[a] Department of Gas Engineering, College of Pipeline and Civil Engineering, China University of Petroleum (East China), Qingdao 266580, China
[b] Department of Chemical and Biomolecular Engineering, National University of Singapore, Singapore

GRAPHICAL ABSTRACT

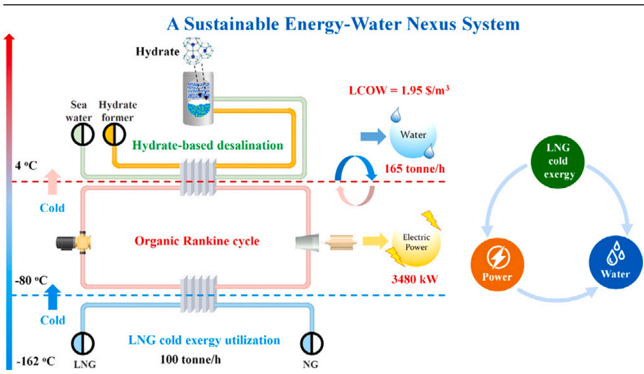

ARTICLE INFO

Keywords:
LNG
Cold exergy
Organic Rankine cycle
Gas hydrate
Desalination

ABSTRACT

Clathrate hydrate-based desalination (HyDesal) is a promising desalination technology but it is energy intensive. Developing strategies to reduce the high energy consumption of HyDesal process is necessary for its industrial application. The need for refrigeration requirement for the operation of HyDesal can be offset by LNG cold exergy to reduce its energy consumption. However, the LNG cold exergy utilization efficiency is low due to the large temperature difference between LNG and seawater and hydrate former. In this work, we propose a sustainable process that integrates HyDesal and organic Rankine cycle by utilizing LNG cold exergy to generate fresh water and electricity simultaneously. This integrated process was optimized by adopting particle swarm optimization algorithm to achieve maximal power and fresh water generation. Further, an economic analysis was performed to compare the economic performance of the proposed system and the base case. The results showed that the proposed process could achieve zero specific energy consumption for desalination and generate extra power. The largest fresh water production and power generation of 165.3 tonne/h and 3480 kW were achieved by adopting cyclopentane as hydrate former and mixed working fluid in organic Rankine cycle based on 100 tonne/h of LNG flowrate. The lowest levelized cost of water of the proposed process was 1.946 $/m^3, which was 21.05% lower than that of the base case. Thus, the proposed sustainable process can strengthen the energy–water nexus and reduce the greenhouse gas emission by utilizing LNG cold exergy.

1. Introduction

The demand for clean energy has increased significantly in the world including China. Up to 2018, coal accounts for 59% of the

* Corresponding authors.
E-mail addresses: hetianbiao@upc.edu.cn (T. He), praveen.linga@nus.edu.sg (P. Linga).

https://doi.org/10.1016/j.apenergy.2021.116839
Received 25 November 2020; Received in revised form 3 March 2021; Accepted 16 March 2021

Nomenclature

Acronym

C	Compressor
DCC	Direct capital cost
E	Expander
EG	Ethylene glycol
FCI	Fixed capital investment
HEX	Heat exchanger
HF	Hydrate former
IC	Insurance cost
ICC	Indirect capital cost
LCOW	Levelized cost of water
LMTD	Log mean temperature difference
LNG	Liquefied natural gas
MTA	Minimum temperature approach
NG	Natural gas
OC	Operation and maintenance cost
ORC	Organic Rankine cycle
P	Pump
PR	Pressure ratio
PSO	Particle swarm optimization
SW	Seawater
TCC	Total capital cost
VF	Vapor fraction

Symbols

α	Capital recovery factor
β	Construction factor
$\dot{E}$	Exergy, kW
$\dot{m}$	Mass flowrate, kg/h
$\dot{n}$	Molar flowrate, kmol/h
$\dot{W}$	Power, kW
η	Exergetic efficiency
e	Specific exergy, kW/kg
h	Specific enthalpy, kJ/kg
i	Interest rate
P	Pressure, kPa
Q	Volumetric flow, m^3
r_n	Nominal escalation factor
s	Specific entropy, kJ/(kg K)
T	Temperature, °C
X	Decision variables vector
x	Molar fraction

Subscripts

0	Dead state
BM	Bare module
c	Compressor
$cont$	Contingency
d	Destruction
e	Expander
in	Inlet
net	Net power
out	Outlet
P	Purchased
p	Pump
$total$	Total
u	Utilized

primary energy consumption in China, while natural gas only contributes less than 7.8% which is substantially lower than the average natural gas percentage of 24% in the world [1]. Natural gas as one of the cleanest fossil fuels will become a hot spot of the global energy consumption in the future [2].

Due to the natural gas scarcity in China, around 25 liquefied natural gas (LNG) regasification terminals have been built in the coastal areas to import LNG from other countries [3]. LNG cannot be utilized before it is vaporized with the external heating [4]. During the vaporization process, there is around 850 kJ/kg of cold exergy released to the seawater in LNG vaporizers when LNG is heated from −162 °C to 25 °C at 1 atm [5]. It is reported that the LNG regasification capacity around the world comes to 826 million tonnes per annum (MTPA) in 2020 [6]. Thus, the available LNG cold exergy reaches 6.855×10^{14} kJ per year (21 739.9 MW). If we can convert 30% of the total LNG cold exergy to power, it is almost equivalent to the power generation capacity of the largest coal power plant (Tuoketuo power plant, 6720 MW) in the world [7]. This can save around 1.7×10^{17} tonnes coal per year and reduce huge amounts of greenhouse gas emission and NOx which is essential to make a sustainable society [8]. However, most of the LNG cold exergy is wasted which reduces the overall energy efficiency of the regasification process.

There are several methods to utilize LNG cold exergy, including desalination [9], power generation [10], air separation [11], cryogenic carbon dioxide capture [12], and inlet air cooling [13,14], etc. Up to now, LNG cold exergy utilization adopts single method, in which applying organic Rankine cycle (ORC) for power generation is the most widely used one. Zhang and Lior [15] designed a supercritical carbon dioxide Rankine cycle combined with a conventional Brayton cycle to harvest the LNG cold exergy. The results implied that the energy and exergy efficiency was 65% and 50%, respectively. Shi and Che [16] adopted Rankine cycle using water and ammonia mixed working fluid to recover the waste heat and LNG cold exergy which resulted in 48% of the exergy efficiency. Querol et al. [17] suggested that ammonia Rankine cycle could be integrated with LNG vaporization process to harness LNG cold exergy because of its lower thermoeconomic cost. Lee et al. [18] designed a combined CO_2 Rankine cycle to recover the LNG cold exergy and the waste heat from the coal power plant. García et al. [19] proposed two Rankine cycles (adopting CH_4 and Ar as the working fluid) placed in cascade and integrated with direct expansion to use LNG cold exergy. The specific power generation was 235 kW/kg of LNG with the minimum temperature approach of 2 K. Ghaebi et al. [20] conducted 3E (energy, exergy, and economic) investigation on a novel ammonia-water mixed working fluid Rankine cycle for power and cooling cogeneration by utilizing LNG as the heat sink. The net output power and exergy efficiency were 1378 kW and 22.51%, respectively. Bao et al. [21] studied the effects of the configuration of pumps and expanders in two-stage condensation ORC on net power output and thermodynamic efficiency. ORC is a good option to recover LNG cold exergy in the low-temperature range with relatively high efficiency. However, it is of low efficiency to utilize the LNG cold exergy in the high-temperature range. Sun et al. [22] optimized three different ORC configurations to utilize LNG cold exergy. They found that the two-stage parallel ORC with ammonia-ethane as its working fluid achieved the highest exergy efficiency of 17.36%. Then, they [23] proposed three different two-stage ORCs to optimize their working fluids. The best thermodynamic and economic performance was obtained by two-stage condensation ORC.

Fresh water scarcity has been a global challenge, and desalination technologies acquire numerous spotlight on producing sufficient fresh water from sea water. Hydrate-based desalination process (HyDesal) uses guest gases or liquids to induce water forming hydrate crystal to capture the guest molecular and exclude salts [24]. Afterward, hydrate crystal is separated from the seawater and dissociated into fresh water and guest molecular [25]. Propane [26] and cyclopentane [27] are considered as potential hydrate formers for the HyDesal process due to their mild formation conditions. Zheng and Yang [28] conducted experiments on a novel gas hydrate-based desalination system under different separation modes. The results showed that the desalination efficiency was higher than 80%. Moreover, a high pressure hydrate-based desalination experiment with a high pressure visual cell obtained up to 80% of desalination efficiencies [29]. The energy consumption of HyDesal is lower than that of freeze desalination because the hydrate formation temperature is higher than the ice point temperature. Moreover, its energy consumption can be further reduced by utilizing the LNG cold exergy. He et al. proposed a novel process by integrating HyDesal with LNG cold exergy utilization (ColdEn-HyDesal) by adopting propane [30] and cyclopentane [31] as the hydrate former which reduced the specific energy consumption of HyDesal from 65.13 kWh/m^3 to 0.84 kWh/m^3 and 0.35 kWh/m^3, respectively. Chong et al. [32] investigated the economic performance of the ColdEn-HyDesal process. They found out that the levelized cost of water (LCOW) reduced from 9.31 $\$/m^3$ (without LNG cold exergy) to 1.11 $\$/m^3$ (using LNG cold exergy). Moreover, the LCOW of the ColdEn-HyDesal process was lower than other desalination technologies when the plant capacity was larger than 5×10^4 m^3. This indicated that the energy and economic performance of the HyDesal process could be enhanced significantly by utilizing the LNG cold exergy.

According to the above literature review, it can be seen that the high energy and exergy efficiency of the ORC to recover LNG cold exergy is achieved when the waste heat is available as the heat source. However, the waste heat is not accessible in most LNG regasification terminals where the sea water is the main heat source. Thus, it is crucial to obtain the optimal design parameters of the ORC system adopting LNG as the heat sink and low temperature heat source. Moreover, only using ORC to recover the LNG cold exergy is of low efficiency especially in the high-temperature range where the working fluid condensation curve is hard to match the LNG single phase heating curve. For the case of HyDesal process, the large temperature difference between LNG and other streams (i.e. guest gas and sea water) results in 10.71% of the exergy efficiency [31]. The large exergy destruction in the HyDesal process by utilizing LNG cold exergy directly makes a promising chance for process integration to improve the overall exergy efficiency. Apart from the refrigeration requirement of the HyDesal process, the energy consumption is also the main obstacle to its widely application. Therefore, it is necessary to integrate the HyDesal process with other power generation systems to reduce its specific energy consumption and increase the exergy efficiency by introducing a heat transfer medium between LNG and guest gas and sea water. To the best of our knowledge, there is lack of study focusing on designing and optimizing the HyDesal process integrated with power generation cycles by utilizing the LNG cold exergy in the open literature. It is also imperative to utilize the waste LNG cold exergy for clean power generation and fresh water production to reduce the greenhouse gas emissions and achieve carbon neutral. Hence, it is vital to address these research gaps to propose a novel sustainable system integrating the ORC with HyDesal by utilizing the LNG cold exergy to produce power and fresh water simultaneously.

In this paper, an ORC integrated with HyDesal process by utilizing LNG cold exergy (ColdEn-HyDesal-ORC) was proposed to improve the LNG cold exergy utilization efficiency and achieve sustainable power and fresh water production. The LNG cold exergy is recovered by ORC and HyDesal subsystems successively. The ORC working fluid transfers the LNG cooling capacity to the hydrate former and seawater to meet the refrigeration requirement in the HyDesal subsystem. In addition, the power generated by ORC can drive the compressors and pumps in HyDesal subsystem which can achieve zero specific energy consumption of the fresh water production. To solve two main challenges faced by the world, namely clean energy and fresh water scarcity, by harnessing the wasted LNG cold exergy is crucial for building a sustainable society. This study offers some important insights into how to establish the energy and water connection based on existing technologies and industrial processes.

2. Process design and input parameters

2.1. ColdEn-HyDesal-ORC process description

The flowsheet of the ColdEn-HyDesal-ORC process using propane (ColdEn-HyDesal(C_3H_8)-ORC) and cyclopentane (CP) (ColdEn-HyDesal (CP)-ORC) as hydrate former is illustrated in Figs. 1 and 2, respectively. The low-temperature LNG cold exergy is recovered by the ORC working fluid in the condenser (HEX-7). Then, the seawater for desalination utilizes the high-temperature LNG cold exergy in HEX-6. After releasing its cold exergy, LNG converts from liquid phase to gaseous phase and enters into the natural gas pipeline for distribution. The working fluid (stream F6) of the ORC is condensed by LNG and then pressurized to the evaporation pressure in pump (P-4). Afterward, the working fluid evaporates by absorbing heats in HEX-1, HEX-2 and HEX-3 successively. The vapor working fluid generates mechanical power in expander by reducing its pressure.

In HyDesal subsystem, the feed seawater is pumped to hydrate formation pressure and then precooled by brine and fresh water in HEX-4 and HEX-5, respectively. Then it is cooled to hydrate formation temperature by the ORC working fluid and LNG successively and enters the hydrate formation reactor. The hydrate former (propane and cyclopentane) is pressurized and then enters the reactor after being cooled by ORC working fluid in HEX-2. When the hydrate formation reaction finishes, the hydrate crystal is separated from the liquid–solid mixture in a three-phase separator. Then the hydrate is dissociated into fresh water and hydrate former by heat stimulation. Since the hydrate formation is exothermic, ethylene glycol as the coolant is applied to remove the reaction heat from the reactor to keep the desired temperature. The ethylene glycol releases the reaction heat to ORC working fluid in HEX-1.

The power generated by the expander in the ORC can be used to drive the hydrate former compressor and four pumps. Therefore, zero energy consumption for fresh water production and extra power output are achieved to nexus power and water in a sustainable way.

2.2. Simulation parameters and assumptions

The flowrate of LNG is set as 100 tonne/h which is equal to the daily regasification capacity of a middle-scale LNG terminal. The temperature, pressure and composition of the feed LNG are listed in Table 1. Propane and CP are selected as the hydrate former due to their mild hydrate formation conditions which can reduce the energy consumption of desalination. The formation and dissociation conditions for propane hydrate are 1 °C, 400 kPa and 6.5 °C, 400 kPa [30], respectively. Moreover, those for CP hydrate are 4 °C, 101.325 kPa and 10 °C, 101.325 kPa [31], respectively.

The working fluid selection for the ORC has a significant influence on the net power output and the overall thermodynamic efficiency. In this study, several single working fluids and one mixed working fluid are adopted to compare their performance in terms of net power output and exergy efficiency, as shown in Table 2.

The ColdEn-HyDesal-ORC process is modeled in Aspen HYSYS V10.0 [33], a mature commercial process simulator. The Peng–Robinson equation of state [34] is adopted to calculate the thermodynamic properties. Several assumptions are proposed to simplify the simulation, as shown below:

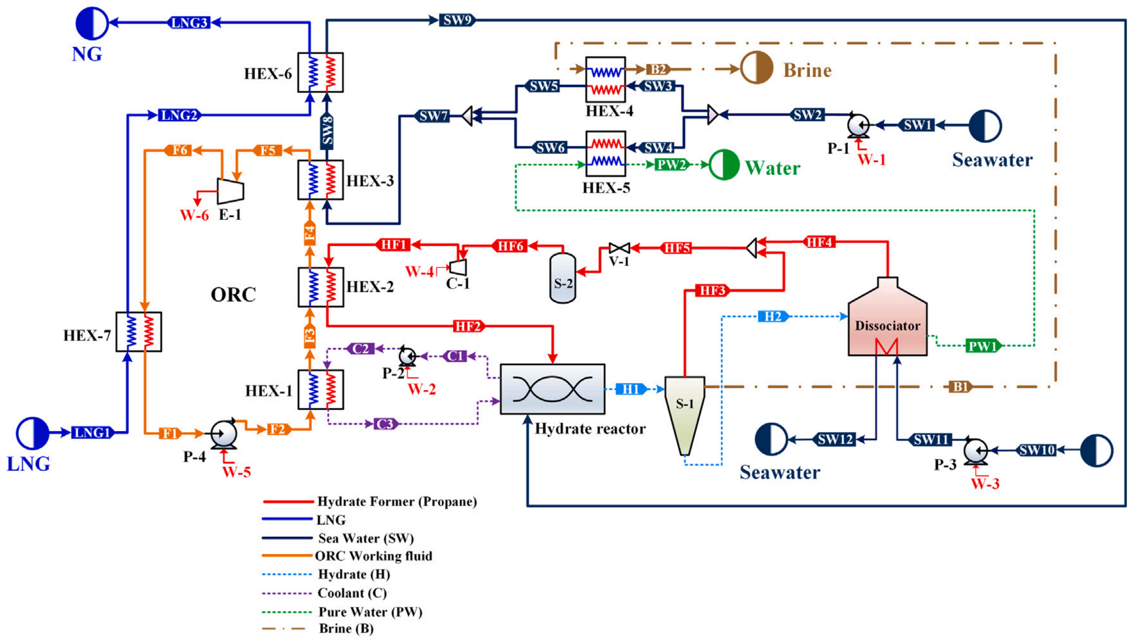

Fig. 1. Flowsheet of the ColdEn-HyDesal(C_3H_8)-ORC process.

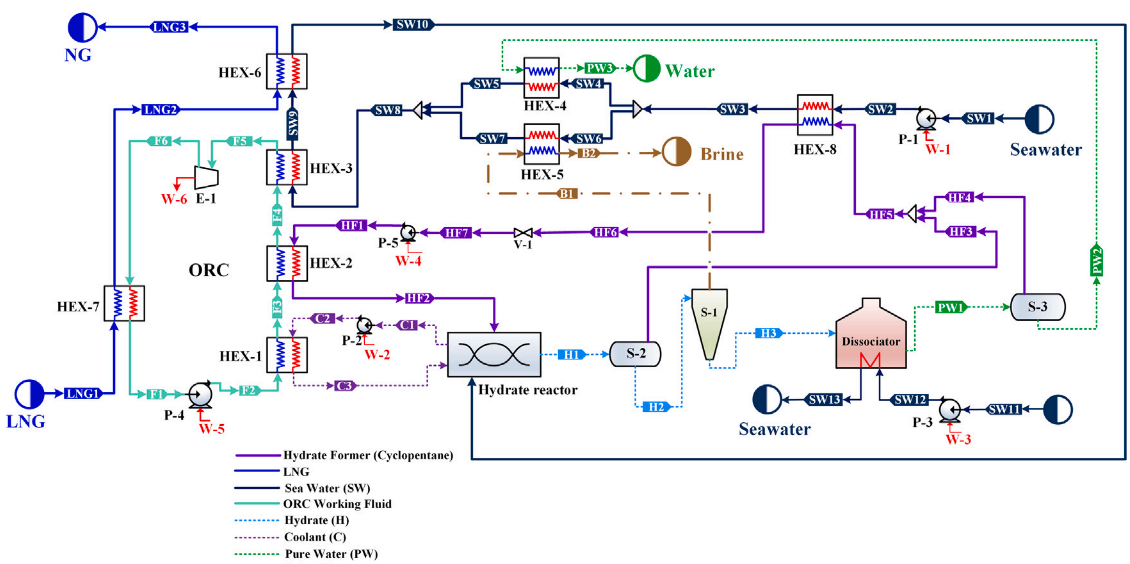

Fig. 2. Flowsheet of the ColdEn-HyDesal(CP)-ORC process.

Table 1
The condition of the feed LNG [30].

Parameters	Values
Temperature (°C)	−159.7
Pressure (kPa)	4400
Molar fraction	
CH_4	0.9934
C_2H_6	0.0051
N_2	0.0015

1. The simulation is in steady-state.
2. The adiabatic efficiencies of pump, compressor, and expander are 75%, 75%, and 80%, respectively.
3. The water recovery rate of propane and CP is 40% and 40% in one hour, respectively. The dissociation conversion rate is 100% [30].
4. The molar flow rate of hydrate former and water is 1:17.

3. Simulation-based optimization

3.1. Objective function and optimization algorithm

The proposed ColdEn-HyDesal-ORC process can achieve zero energy consumption for desalination and generate extra power. The net output power can be expressed in Eq. (1).

$$\dot{W}_{net} = \dot{W}_e - \sum \dot{W}_p - \dot{W}_c \tag{1}$$

Table 2
The potential working fluids for the ORC.

Name	Chemical formula	Normal boiling point (°C)	ODP	GWP (100 years)
Ethylene	C_2H_4	−103.8	0.000	3.700
Ethane	C_2H_6	−88.82	0.000	5.500
R32	CH_2F_2	−51.65	0.000	550.0
Ethane/Propane	C_2H_6/C_3H_8	–	0.000	–

Table 3
The tuning parameters of the PSO [41].

Parameters	Values
Swarm size	100
Function tolerance	10^{-6}
Hybrid function	@fmincon
Max stall iterations	20
Min neighbors fraction	0.25
Self adjustment weight	1.49
Social adjustment weight	1.49

Table 4
The lower and upper bounds of the decision parameters.

Parameters	Lower bound	Upper bound
$\dot{m}_{F1}$ (kg/s)	2.778	55.56
x	0	1
P_{F2} (kPa)	500.0	2500
P_{F6} (kPa)	106.0	500.0
T_{F5} (°C)	0.000	20.00
$\dot{m}_{HF1}$ (kg/s)	8.333	69.44

where $\dot{W}_{net}$ is the net output power of ColdEn-HyDesal-ORC process, kW; $\dot{W}_e$ is the expansion output power of the ORC, kW; $\dot{W}_p$ refers to the power consumption of pumps, kW; $\dot{W}_c$ denotes the power consumption of guest gas compressor, kW.

Due to highly nonlinear and non-convex equations used to express thermodynamic properties, optimization of the proposed system and similar LNG related systems is difficult for deterministic optimization algorithms. Thus, stochastic optimization algorithms are the best option to solve the problem [35]. Particle swarm optimization algorithm (PSO) is a stochastic optimization algorithm simulating a group of birds looking for food to obtain the optimal results [36]. The PSO and genetic algorithm (GA) are the most widely used stochastic optimization algorithms in LNG related processes due to their mature and easy to implement. It was reported that PSO was evolved to rectify the challenges faced in GA including large number of tuning parameters [37] and bad computational efficiency [38]. The main advantages of the PSO include small amount of parameters needed to be tuned and non-gradient dependence [39], making it suitable for the highly nonlinear optimization problem, i.e. LNG cold exergy utilization system adopting mixed working fluid [23]. Therefore, the PSO implemented in MATLAB [40] is adopted to optimize the proposed process and the tuning parameters are listed in Table 3. Aspen HYSYS can interact its data with Matlab by ActiveX, as shown in Fig. 3.

The decision variables will affect the overall performance of the ColdEn-HyDesal-ORC process. In the ORC subsystem, the working fluid components, the mass flowrate, evaporation pressure, and condensation pressure have significant influence on the power output. Moreover, since there are three evaporators in the ORC, the output temperature of the third-stage evaporator (HEX-3) also affects the power output of the expander. In the HyDesal subsystem, the mass flowrate of the hydrate former not only affects the production capacity of the fresh water, but also impacts the net power output. It is because the mass flowrate of the hydrate former determines the reaction heat in the hydrate formation reactor which is released to the ORC working fluid. The increase of the reaction heat makes a smaller net power output. Thus, the decision variable vector X including the mass flowrate, molar fraction, evaporation pressure, evaporation temperature, condensation pressure of the working fluid in ORC and the mass flowrate of the hydrate former is defined in Eq. (2). It should be noted that the molar fraction of the working fluid is only optimized for the mixed working fluid. The lower and upper bounds of the decision parameters are shown in Table 4.

$$X = [\dot{m}_{F1}, x, P_{F2}, P_{F6}, T_{F5}, \dot{m}_{HF1}] \tag{2}$$

The objective function of this study is to maximize the net output power, as defined in Eq. (3). It should be noted that almost 70% of the refrigeration requirement in the HyDesal process is provided by the ORC working fluid in evaporators. In the proposed system, the ORC working fluid can be treated as the intermediate medium to transfer the refrigeration capacity from the LNG to the HyDesal process. Thus, to maximize the power output is equivalent to maximize hydrate former and seawater flowrates for hydrate formation and thereby maximize the fresh water production.

$$max[f(X)] = \dot{W}_{net} \tag{3}$$

3.2. Constraints and penalty function

It is crucial to set several constraints to prevent the algorithm searching beyond the feasible range. For most of energy related processes, the internal temperature cross in heat exchangers should be avoided. In this study, three constraints are proposed, as shown below:

1. The minimum temperature approach (MTA) of heat exchangers should be equal to or larger than 2 °C to provide enough driving force for heat transfer, as described in Eq. (4).

$$c_1(X) = MTA - 2 \geq 0 \tag{4}$$

2. The working fluid of ORC should be superheated before entering the expander to prevent the liquid strike on the blades. Thus, the vapor fraction (VF) of the stream should be equal to 1, which can be defined in Eq. (5).

$$c_2(X) = VF - 1 = 0 \tag{5}$$

3. The outlet temperature of the natural gas for distribution should be larger than 5 °C, as shown in Eq. (6).

$$c_3(X) = T_{LNG3} - 5 \geq 0 \tag{6}$$

Penalty function is applied to replace the objective function when the constraints are violated, as described in Eq. (7). Since the objective function is to maximize the net output power, the penalty function returns an extremely small number which leads to the algorithm abandoning this particle.

$$p(X) = -100 \times exp^{max\left[\left|\frac{c_1(X)}{2}\right|, \left|\frac{c_2(X)}{1}\right|, \left|\frac{c_3(X)}{5}\right|\right]} \times \dot{W}_{net} \tag{7}$$

where $c_1(X)$, $c_2(X)$, and $c_2(X)$ is divided by 2 °C, 1, and 5 °C, respectively, to make them unit-less and comparable in the function of *max*.

4. Results and discussion

4.1. Optimization results

The optimized case 1, 2, 3, and 4 adopt R32, ethylene, ethane, and ethane/propane binary mixture as working fluid in the ORC,

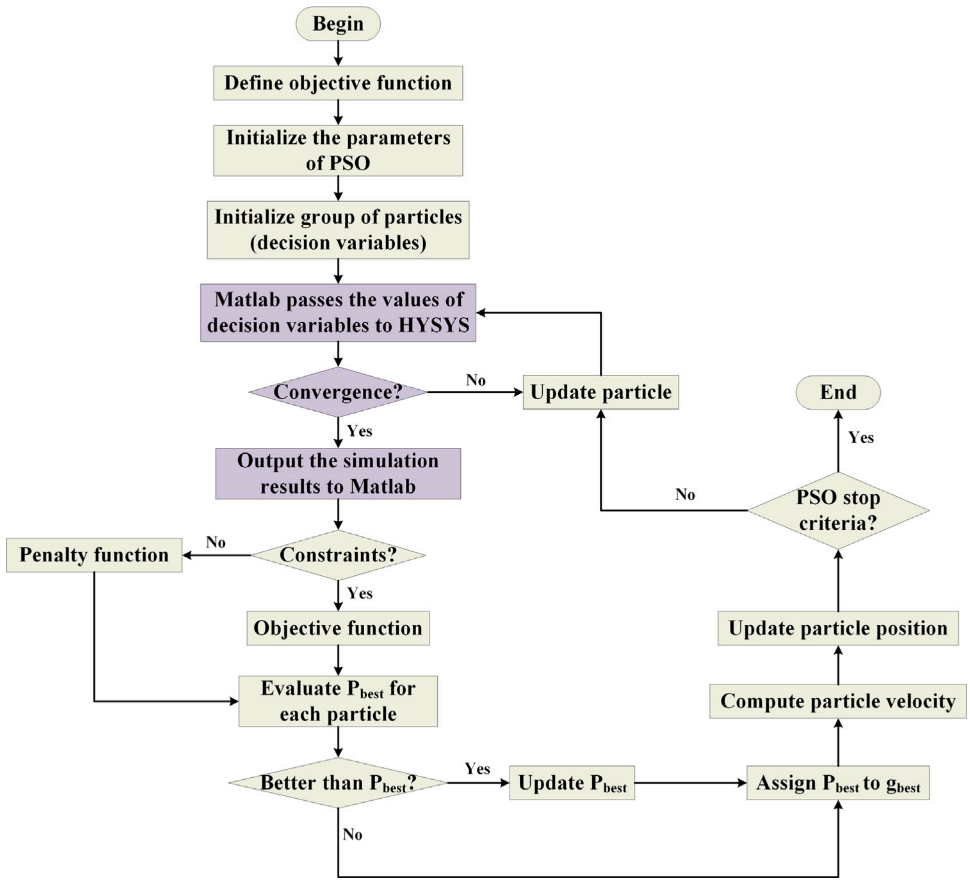

Fig. 3. Optimization flowchart of ColdEn-HyDesal-ORC process.

respectively, where propane is used as the hydrate former in these four cases. However, CP is selected as the hydrate former in the optimized case 5, 6, 7, and 8 where R32, ethylene, ethane, and ethane/propane binary mixture is utilized as the working fluid in the ORC subsystem, respectively. Totally eight optimized cases were obtained by adopting PSO to optimize their respective decision variables. The optimization results of the ColdEn-HyDesal(C_3H_8)-ORC process were shown in Table 5. For the optimized case 1, the mass flowrate of R32 was the largest among four different working fluids, while the mass flowrate of the guest gas was the smallest. Moreover, the evaporation and condensation pressure were 586 kPa and 106 kPa, respectively, which were also the lowest among the four cases. When ethylene was adopted as the working fluid of the ORC, the mass flowrate of ethylene decreased from 41.98 kg/s to 31.76 kg/s compared to R32. The mass flowrate of the hydrate former increased from 13.99 kg/s to 14.16 kg/s which can generate more fresh water. For the optimized case 3, the mass flowrate of ethane and hydrate former increased from 31.76 kg/s to 38.79 kg/s and 14.16 kg/s to 14.22 kg/s compared to the optimized case 2, respectively. For the optimized case 4, the optimal molar fractions of the mixed working fluid were 0.8617 of ethane and 0.1383 of propane. The mass flowrate of the mixed working fluid was 8.82% lower than that of ethane, while the mass flowrate of the hydrate former was 2.58% higher than that of ethane. However, the pressure ratio of the mixed working fluid was 7.58 which was the highest among four cases.

Table 6 showed the optimal decision variables of the ColdEn-HyDesal(CP)-ORC process. When CP was adopted as the hydrate former, the mass flow rate of the hydrate former increased, while the pressure ratio of the ORC decreased from the optimized cases 5 to 8. For the optimized case 8, the optimal molar fraction of the working fluid of the ORC was 0.9011 of ethane and 0.09889 of propane, which was different with the optimized case 4 using propane as the hydrate former.

Tables 7 and 8 illustrated the fresh water flowrates and net output powers of the ColdEn-HyDesal-ORC process using propane and CP as hydrate former after the optimization by PSO, respectively. For the ColdEn-HyDesal(C_3H_8)-ORC process, it was clear that the fresh water flowrate of the optimized case 4 adopting mixed working fluid was 145.7 tonne/h, which was 4.19%, 2.98%, and 2.58% higher than that of the optimized case 1, 2, and 3, respectively. Moreover, the net output power of the optimized case 4 was 2931 kW, which was 49.69%, 30.15%, and 25.72% higher than that of the optimized case 1, 2, and 3, respectively. For the ColdEn-HyDesal(CP)-ORC process, the largest fresh water flowrate of 165.3 tonne/h was achieved by the optimized case 8 by using mixed working fluid, which was 6.67%, 5.19%, and 2.96% higher than that of the optimized case 5, 6, and 7, respectively. The net power output of the optimized case 8 was 3480.18 kW, which was 32.69%, 23.95%, and 9.71% higher than that of the optimized case 5, 6, and 7, respectively. These results indicated that utilizing mixed working fluid in the ColdEn-HyDesal-ORC process could generate more fresh water and net output power. Thus, it was crucial to adopt mixed working fluid in the ORC to recover the LNG cold energy. Among the eight cases, the largest net power output and fresh water flowrate were achieved by the optimized case 8 using CP as hydrate former and mixed working fluid in ORC. The net power output and fresh water flowrate of the optimized case 8 was 18.75% and 13.45% higher than the optimized case 4, respectively. The optimal material streams of the optimized case 4 and 8 were summarized in Tables A.1 and A.2, respectively.

4.2. Composite curves analysis

The heat transfer between LNG and hot streams can reflect the LNG cold exergy utilization efficiency. Figs. 4 and 5 demonstrated the heat

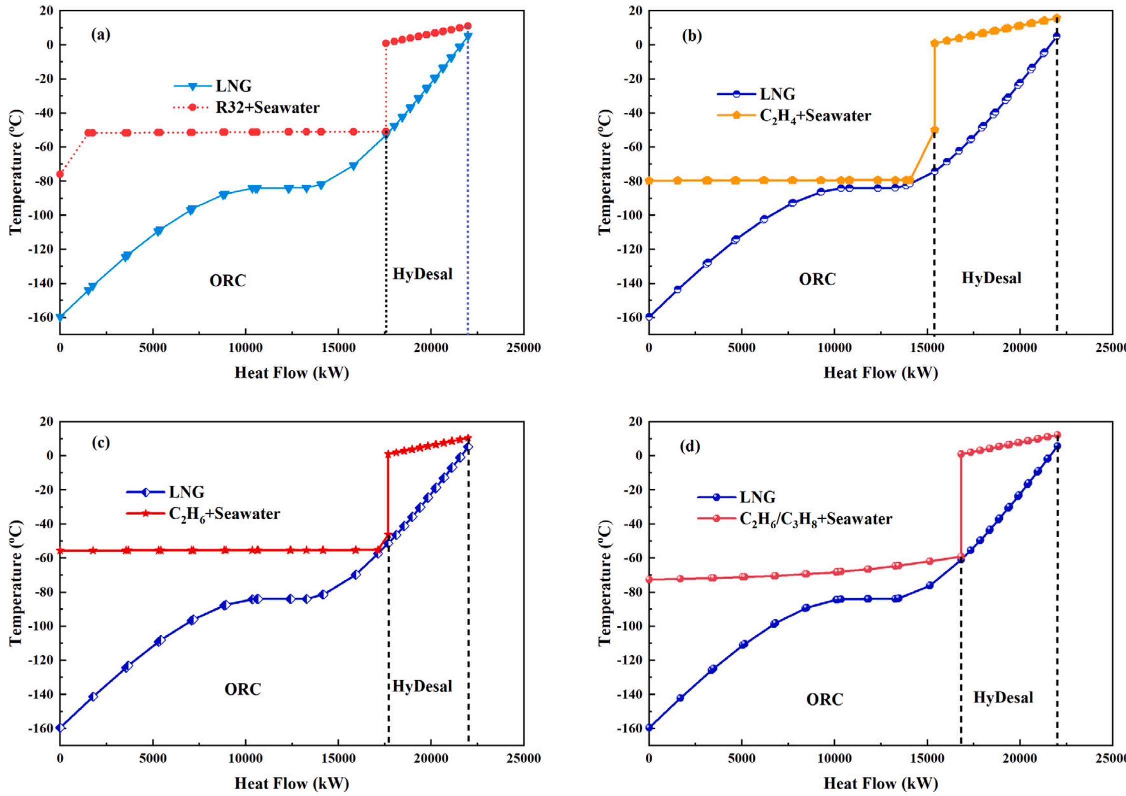

Fig. 4. Heat transfer curve between LNG and hot streams (a) Optimized case 1, (b) Optimized case 2, (c) Optimized case 3, (d) Optimized case 4.

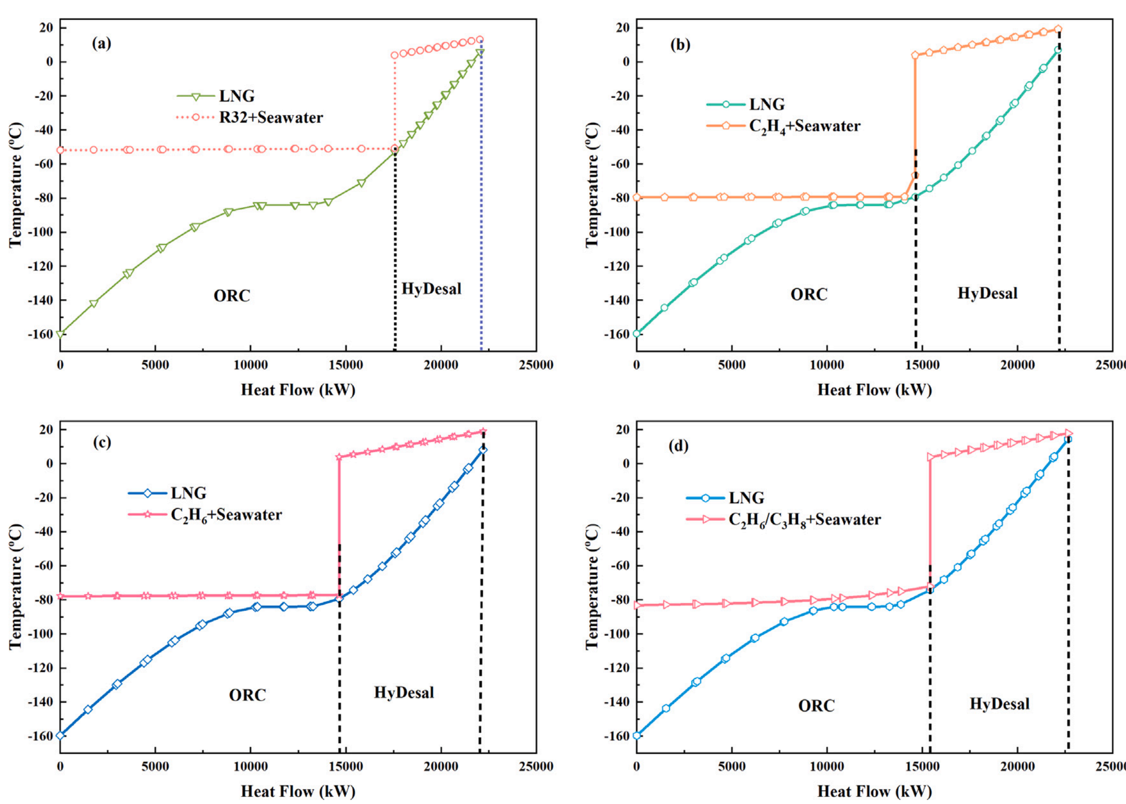

Fig. 5. Heat transfer curve between LNG and hot streams (a) Optimized case 5, (b) Optimized case 6, (c) Optimized case 7, (d) Optimized case 8.

Table 5
Optimization results of the decision variables of the ColdEn-HyDesal(C_3H_8)-ORC process.

Variables	Optimized case 1	Optimized case 2	Optimized case 3	Optimized case 4
$\dot{m}_{F1}$ (kg/s)	41.98	31.76	38.79	35.36
x	$x_{R32} = 1.000$	$x_{C_2H_4} = 1.000$	$x_{C_2H_6} = 1.000$	$x_{C_2H_6}/x_{C_3H_8} = 0.8617/0.1383$
P_{F2} (kPa)	586.0	1499	1874	1510
P_{F6} (kPa)	106.0	351.0	455.0	199.0
T_{F5} (°C)	14.99	16.00	14.31	12.72
$\dot{m}_{HF1}$ (kg/s)	13.99	14.16	14.22	14.59

Table 6
Optimization results of the decision variables of the ColdEn-HyDesal(CP)-ORC process.

Variables	Optimized case 5	Optimized case 6	Optimized case 7	Optimized case 8
$\dot{m}_{F1}$ (kg/s)	46.30	31.76	30.91	32.33
x	$x_{R32} = 1.000$	$x_{C_2H_4} = 1.000$	$x_{C_2H_6} = 1.000$	$x_{C_2H_6}/x_{C_3H_8} = 0.9011/0.09889$
P_{F2} (kPa)	641.0	2160	2004	1765
P_{F6} (kPa)	106.0	354.0	181.0	128.0
T_{F5} (°C)	15.06	17.00	16.98	14.90
$\dot{m}_{HF1}$ (kg/s)	24.54	24.93	25.52	26.30

Table 7
Fresh water flowrate and net output power of the ColdEn-HyDesal(C_3H_8)-ORC process.

Parameters	Optimized case 1	Optimized case 2	Optimized case 3	Optimized case 4
$\dot{m}_{PW\text{-}1}$ (tonne/h)	139.9	141.5	142.1	145.7
$\dot{W}_1$ (kW)	40.03	40.50	40.66	41.71
$\dot{W}_2$ (kW)	8.429	8.529	8.559	8.779
$\dot{W}_3$ (kW)	33.03	33.42	33.55	34.41
$\dot{W}_4$ (kW)	33.70	34.10	34.23	35.11
$\dot{W}_5$ (kW)	21.46	91.88	147.0	115.4
$\dot{W}_6$ (kW)	2094	2460	2595	3166
$\dot{W}_{net}$ (kW)	1958	2252	2331	2931

Table 8
Fresh water flowrate and net output power of the ColdEn-HyDesal(CP)-ORC process.

Parameters	Optimized case 5	Optimized case 6	Optimized case 7	Optimized case 8
$\dot{m}_{PW\text{-}1}$ (tonne/h)	154.3	156.8	160.4	165.3
$\dot{W}_1$ (kW)	2.809	2.859	2.919	3.009
$\dot{W}_2$ (kW)	8.219	8.349	8.549	8.809
$\dot{W}_3$ (kW)	32.57	33.09	33.86	34.90
$\dot{W}_4$ (kW)	0.4299	0.4399	0.4499	0.4699
$\dot{W}_5$ (kW)	27.74	144.4	141.7	130.9
$\dot{W}_6$ (kW)	2414	2836	3330	3658
$\dot{W}_{net}$ (kW)	2342	2647	3142	3480

transfer curves of LNG with different ORC working fluids and seawater in HEX-7 and HEX-6 of the ColdEn-HyDesal(C_3H_8)-ORC process and ColdEn-HyDesal(CP)-ORC process, respectively. Since the trends in Figs. 4 and 5 were similar, the following analyze used Fig. 4 as an example. According to Fig. 4(a), the average temperature difference between the cold stream (LNG) and hot stream (R32) in the low-temperature range was the largest due to the high evaporation temperature of R32 (around −50 °C). The log mean temperature difference of HEX-7 and HEX-6 in the optimized case 1 was 29.35 °C and 22.23 °C, respectively. In addition, R32 was subcooled in HEX-7 which reduced the pump power consumption. The LNG cold exergy directly utilized for power generation and hydrate-based desalination were 79.90% and 20.10%, respectively.

From Fig. 4(b), it can be seen that the condensation curve of ethylene and evaporation curve of LNG matched quite well in the temperature range of −90 to −80 °C. This resulted in 9.63 °C of the log mean temperature difference in HEX-7. However, the outlet temperature of LNG from HEX-7 was −74.16 °C which was extremely low to cool the seawater. Thus, the large log mean temperature difference of HEX-6 (35.60 °C) and 29.95% of the LNG cold exergy directly utilized for desalination lead to the low thermodynamic efficiency of the overall performance. It should be noted that ethylene was superheated before entering HEX-7.

Fig. 4(c) illustrated the heat transfer performance between LNG and ethane and seawater. Due to the constant condensation temperature of the single working fluid, the gap between ethane and LNG was still large. The log mean temperature difference of HEX-7 and HEX-6 was 22.51 °C and 21.24 °C, respectively. The amount of LNG cold exergy utilized for power generation and desalination was 80.45% and 19.55%, respectively.

According to Fig. 4(d), the condensation curve of the mixed working fluid was not flat making it possible to match the LNG evaporation curve in the low-temperature range. The log mean temperature difference of HEX-7 and HEX-6 was 19.51 °C and 25.89 °C, respectively. The LNG cold exergy directly recovered by power generation and desalination was 76.40% and 23.60%, respectively. The amount of LNG cold exergy used for power generation with mixed working fluid was only larger than that of ethylene. However, the net output power of the mixed working fluid was the largest among four cases. It indicated that the mixed working fluid with optimal tuned compositions represented a superior thermodynamic performance. The temperature–entropy diagram of the ORC in the optimized case 4 with mixed working fluid was shown in Fig. 6(a). It was clear that the mixed working fluid was superheated before entering the expander which enlarged the power output of the ORC and enhanced the overall performance of the optimized case 4.

The slopes of the seawater curve in four figures were the same since the inlet and outlet temperature were the same. The seawater curve could extend from the right end to the left with the increase of the seawater mass flowrate. Therefore, more LNG cold exergy was directly utilized by desalination. However, it also reduced the outlet temperature of the LNG from HEX-7 that enlarged the entropy generation between LNG and seawater leading to a relatively low thermodynamic efficiency of the ColdEn-HyDesal(C_3H_8)-ORC process, as shown in Fig. 4(b). Thus, there was a trade-off between the amount of LNG cold exergy utilized for power generation and desalination.

4.3. Exergy analysis

Exergy is defined as the maximum theoretical work output obtained when the system transfers from the specified state to the dead state [42]. The definition of the physical exergy for the material stream can be described in Eq. (8).

$$e = h - h_0 - T_0(s - s_0) \tag{8}$$

where e denotes specific exergy; h and s refer to specific enthalpy and entropy, respectively. The subscript 0 represents the dead state, where is 298.15 K and 101.325 kPa.

For a LNG cold exergy utilization system, the aim is to maximally recover the valuable LNG cold exergy and reduce the exergy destruction. LNG cold exergy utilization efficiency is the key indicator to evaluate LNG cold exergy utilization system, which can be defined as the ratio of the rate of utilized exergy from LNG to the rate of total available LNG cold exergy, as shown in Eq. (9). The rate of total available LNG cold exergy is the rate of exergy difference between the stream LNG-1 and LNG-3. The rate of utilized exergy from LNG refers to the summation of the exergy utilized in HEX-6 and HEX-7.

$$\eta_{ex} = \frac{\dot{E}_u}{\dot{E}_{total}} \tag{9}$$

$$\dot{E}_{total} = \dot{E}_{in} - \dot{E}_{out} = \dot{E}_{LNG1} - \dot{E}_{LNG3} \tag{10}$$

$$\dot{E}_u = \dot{E}_{total} - \dot{E}_d \tag{11}$$

$$\dot{E}_d = \dot{E}_d^{HEX-6} + \dot{E}_d^{HEX-7} \tag{12}$$

$$\dot{E}_d^{HEX-6} = \dot{E}_{LNG2} - \dot{E}_{LNG3} + \dot{E}_{SW9} - \dot{E}_{SW10} \tag{13}$$

$$\dot{E}_d^{HEX-7} = \dot{E}_{LNG1} - \dot{E}_{LNG2} + \dot{E}_{F6} - \dot{E}_{F1} \tag{14}$$

where η_{ex} is LNG cold exergy utilization efficiency; $\dot{E}_{total}$ is the rate of total available exergy provided by the LNG, kW; $\dot{E}_{in}$ is the rate of input exergy of the system, kW; $\dot{E}_{out}$ is the rate of output exergy of the system, kW; $\dot{E}_u$ is the rate of amount of exergy utilized by the system, kW; $\dot{E}_d$ is the rate of exergy destruction caused by thermodynamic irreversibility.

The exergy destructions of HEX-6 and HEX-7 in eight optimized cases were shown in Table 9. It can be seen that the exergy destructions of HEX-6 and HEX-7 in the optimized case 1 were 611.8 kW and 7128 kW, respectively, which accounted for the largest exergy destruction in four cases of the ColdEn-HyDesal(C_3H_8)-ORC process. The exergy destruction of HEX-6 and HEX-7 decreased to 574.4 kW and 6789 kW, respectively in the optimized case 3. This was because of the better match of cold and hot composite curves in the optimized case 3 than that of the optimized case 1. Moreover, the exergy destruction of HEX-6 and HEX-7 further reduced to 856.9 kW and 5340 kW, respectively in the optimized case 4. The total exergy destruction of the optimized case 4 was 19.93% and 15.83% lower than that of the optimized case 1 and 3, respectively. It should be noted that the exergy destruction of HEX-7 was the smallest (4169 kW) in the optimized case 2 due to the smallest gap between the LNG and ethylene in HEX-7. However, the exergy destruction of HEX-6 was the largest (1452 kW) because of the huge temperature difference between LNG and seawater. The total exergy destruction was 5621 kW in the optimized case 2. However, the smallest exergy destruction in terms of the LNG cold exergy utilization in the optimized case 2 did not bring the largest net output power and fresh water production. It can be explained by the exergy destruction in three evaporators in the ORC, as shown in Fig. 7. It was clear that the exergy destruction of HEX-1 in the optimized case 2 was 2833 kW, which was significantly larger than the summation of the exergy destruction of three heat exchangers in other three cases. The reason was that the smallest exergy destruction of HEX-6 and HEX-7 did not provide the best overall performance. Moreover, the summation of the exergy destruction of HEX-1, HEX-2, HEX-3, HEX-6, and HEX-7 in the optimized case 4 was the smallest (7505 kW) in four cases. Thus, the optimized case 4 achieved the largest net output power and fresh water production.

For the ColdEn-HyDesal(CP)-ORC process, the exergy destruction of HEX-7 in the optimized case 5 was 7256 kW, which was the largest among the optimized cases 5 to 8, while that of HEX-6 was the smallest (657.9 kW). This resulted in the largest total exergy destruction among the optimized cases 5 to 8. The smallest total exergy destruction of HEX-6 and HEX-7 was achieved by the optimized case 8 due to the best temperature curve matching, which was 43.41%, 8.53%, and 12.05% lower than that in optimized cases 5, 6, and 7, respectively. Although the total exergy destruction of HEX-6 and HEX-7 in the optimized case 6 was 3.14% lower than that in the optimized case 7, the net power output and fresh water production were smaller than the optimized case 7. That was because the total exergy destruction of three evaporators in the optimized case 6 was significantly larger than that in the optimized case 7, as shown in Fig. 7.

Fig. 8 illustrated the LNG cold exergy utilization efficiency comparison between the ColdEn-HyDesal-ORC and ColdEn-HyDesal processes [30,31]. The total available exergy provided to HEX-6 and HEX-7 by 100 tonne/h of LNG was 14188 kW. As shown in Fig. 8, the exergy utilization efficiency of the ColdEn-HyDesal(C_3H_8) process and the ColdEn-HyDesal(CP) process was only 15.51% and 13.44%, respectively. This indicated that 84.49% and 86.56% of the LNG cold exergy were wasted in ColdEn-HyDesal process due to the large temperature difference between LNG and seawater as well as the hydrate former. However, the exergy utilization efficiency of the optimized case 1 increased to 45.44% which was 29.93% higher than that of ColdEn-HyDesal(C_3H_8) process. It indicated that integrating ORC could improve the LNG cold exergy utilization efficiency dramatically. The optimized case 8 by adopting mixed working fluid in ORC achieved the highest exergy utilization efficiency of 61.11%. Moreover, the optimized case 4 applying mixed working fluid in ORC also demonstrated 56.32% of the exergy utilization efficiency. Considering the net output power, fresh water production, and exergy utilization efficiency simultaneously, the optimized cases 4 and 8 was the optimal solution for the ColdEn-HyDesal(C_3H_8)-ORC process and ColdEn-HyDesal(CP)-ORC process, respectively.

4.4. Economic analysis

In this section, economic analysis was conducted to compare the ColdEn-HyDesal-ORC with the ColdEn-HyDesal [30]. It should be noted that the economic performance was not optimized separately which was results of the energy performance optimization. However, the economic analysis was still vital to unfold whether the integrated process would increase the cost of fresh water. The optimized cases 4 and 8 adopting mixed working fluid in the ORC were selected to represent the ColdEn-HyDesal-ORC process since the net output power and fresh water production were the largest. To compare the economic performance between the proposed process and the base case, it is crucial to explore whether the integration of the ORC with the desalination process will increase the cost of fresh water or not. Thus, the net output power is sold to reduce the operation cost when the cost of fresh water is calculated in this study.

Levelized cost of water (LCOW) is defined as the ratio of the summation of the estimation of capital cost accounting for annual and annual operation & maintenance cost to the annual fresh water production [43], which is adopted as the key indicator to analyze the

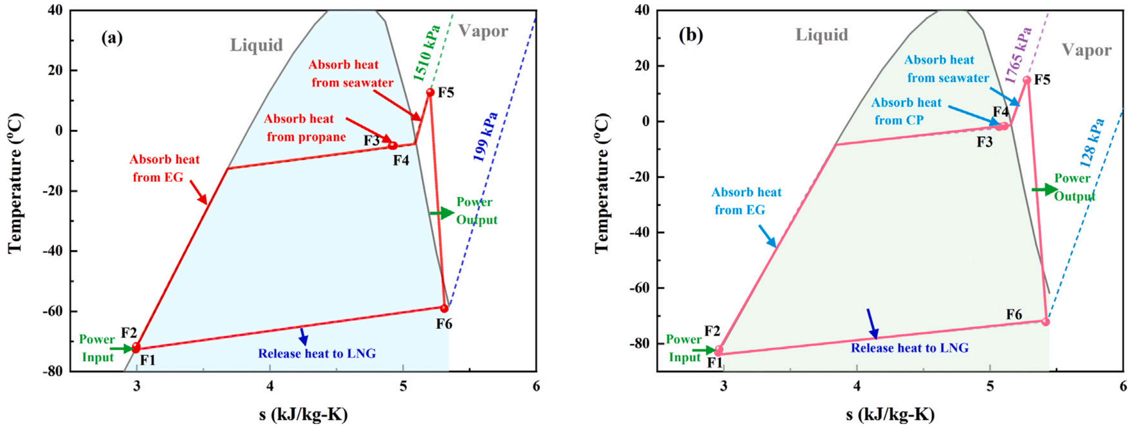

Fig. 6. Temperature–entropy diagram of the ORC: (a) optimized case 4, (b) optimized case 8.

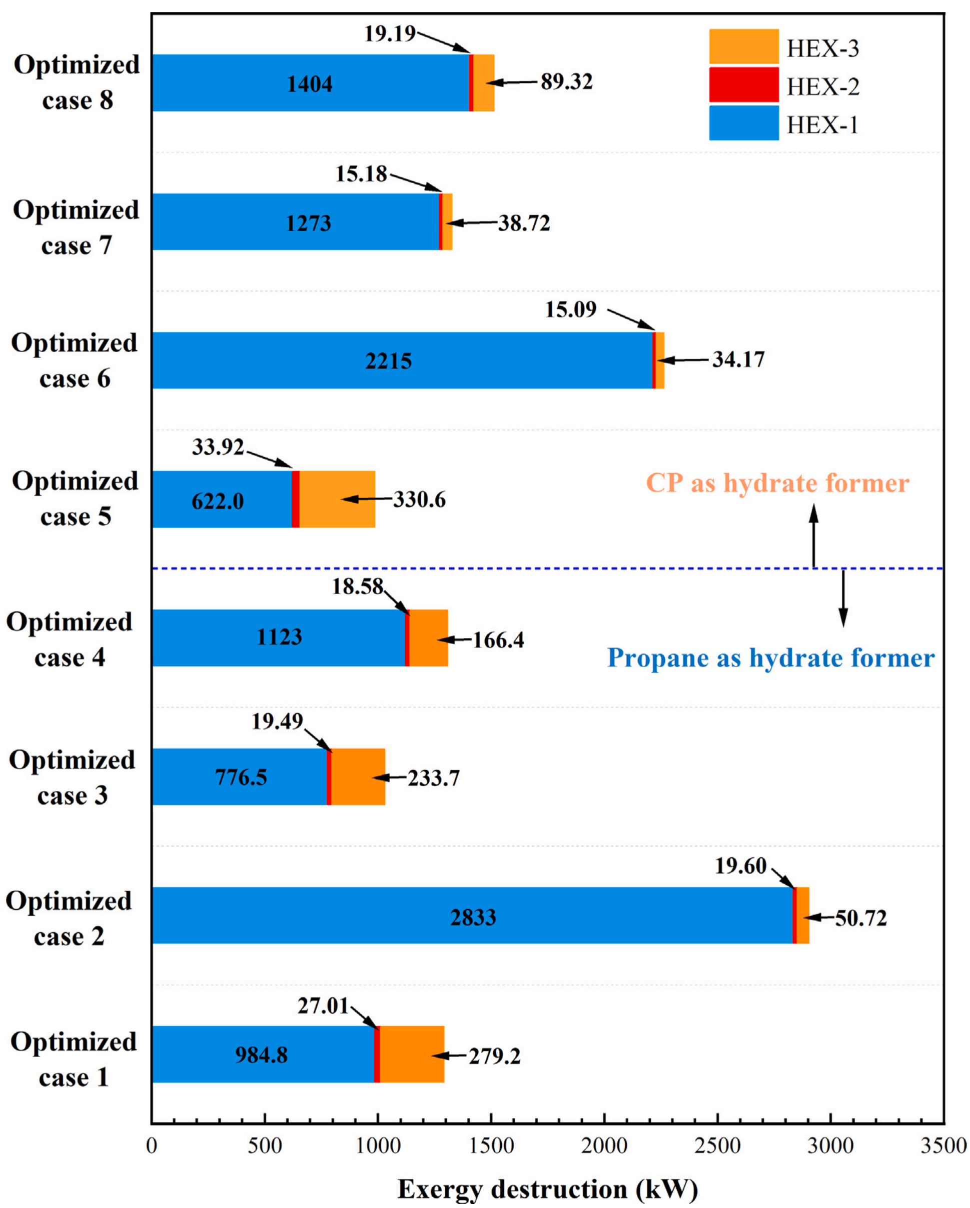

Fig. 7. Exergy destruction of HEX-1, HEX-2, and HEX-3.

Table 9
Exergy destructions of HEX-6 and HEX-7 in four optimized cases.

$\dot{E}_d$	Optimized case 1	Optimized case 2	Optimized case 3	Optimized case 4
HEX-6 (kW)	611.8	1452	574.4	856.9
HEX-7 (kW)	7128	4169	6789	5340
Total (kW)	7740	5621	7363	6197
$\dot{E}_d$	Optimized case 5	Optimized case 6	Optimized case 7	Optimized case 8
HEX-6 (kW)	657.9	1900	1892	1517
HEX-7 (kW)	7256	4089	4291	4001
Total (kW)	7914	5989	6183	5518

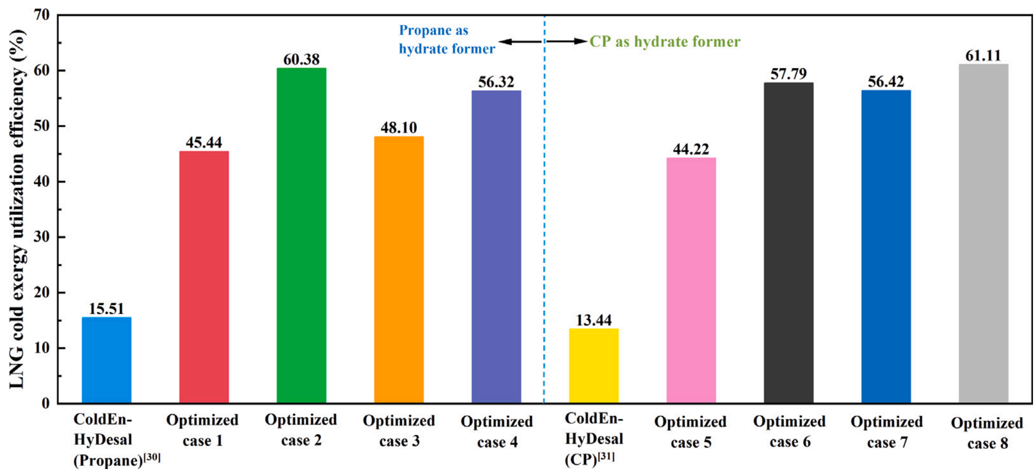

Fig. 8. LNG cold exergy utilization efficiency comparison between eight cases and base cases.

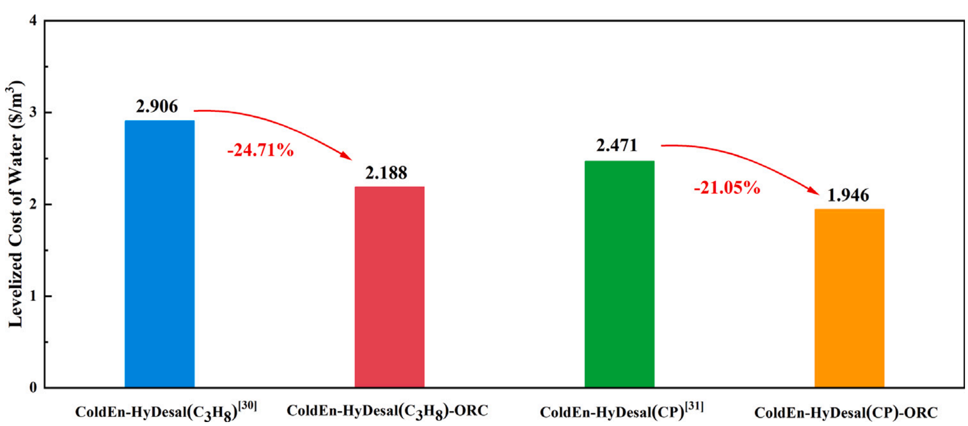

Fig. 9. The levelized cost of water of the ColdEn-HyDesal and ColdEn-HyDesal-ORC processes.

economic performance of the two desalination processes [32], as shown in Eq. (15).

$$LCOW = \frac{\alpha \times FCI + IC + \lambda \times OC}{Q_{water}} \quad (15)$$

where α referred to capital recovery factor, FCI referred to fixed capital investment, IC referred to insurance cost, λ was escalation levelization factor, OC was the operation and maintenance cost, Q_{water} was the annual fresh water production, m^3.

The capital recovery factor α is a ratio used to measure the present value of an annuity by using the lifetime of the plant and the interest rate [44], as defined in Eq. (16).

$$\alpha = \frac{i(1+i)^n}{(1+i)^n - 1} \quad (16)$$

where the interest rate i assumed to be 8%, and the lifetime of the plant n was 25 years.

The escalation levelization factor is employed to reveal the relationship between the first year expenditure value and an equivalent annuity [45], which can be computed from Eqs. (17) and (18) [46].

$$\lambda = \frac{k(1-k^n)}{1-k}\alpha \quad (17)$$

$$k = \frac{1+r_n}{1+i} \quad (18)$$

where r_n was the nominal escalation factor assumed as 2%.

The fixed capital investment (FCI) was the sum of total capital cost (TCC) and contingency cost (C_{cont}), which was presented in Equations (S1) to (S6) in the supplementary material.

Table 10 showed the fixed capital investment, insurance cost and operation & maintenance cost of two processes using different hydrate formers. It can be seen that the fixed capital investment of the ColdEn-HyDesal(C_3H_8)-ORC process was 14.46 million which was 80.05% higher than that of the ColdEn-HyDesal(C_3H_8) process. This was because the cost of the turbine in ORC was very high. In addition, it should be noted that the utilities cost of the ColdEn-HyDesal-ORC was −1.407 million $. The reason was that the ColdEn-HyDesal-ORC

Table 10
Economic analysis between two processes using different hydrate formers.

Cost ($ Million)	ColdEn-HyDesal(C_3H_8) [30]	ColdEn-HyDesal(C_3H_8)-ORC	ColdEn-HyDesal(CP) [31]	ColdEn-HyDesal(CP)-ORC
Total installed cost (TIC)	4.949	8.918	4.526	9.805
Direct capital cost (DCC)	6.286	11.33	5.747	12.45
Indirect capital cost (ICC)	1.014	1.828	0.9277	2.010
Total capital cost (TCC)	7.300	13.15	6.675	14.46
Contingency	0.7300	1.315	0.67	1.446
Fixed capital investment (FCI)	**8.031**	**14.46**	**7.342**	**15.91**
Amortization	0.7523	1.355	0.6878	1.490
Insurance	0.07424	0.1338	0.06788	0.1471
Insurance cost (IC)	**0.8265**	**1.489**	**0.7557**	**1.637**
Operating labor	0.6072	0.6072	0.6072	0.6072
Direct supervisory	0.1093	0.1093	0.1093	0.1093
Utilities	0.1042	−1.407	0.03654	−1.670
Chemical	0.1550	0.1550	0.1550	0.1550
Maintenance	0.09899	0.1784	0.09051	0.1961
Operating supplies	0.02325	0.02325	0.02325	0.02325
Laboratory charges	0.09108	0.09108	0.09108	0.09108
Operation & maintenance cost (OC)	**1.189**	**−0.2425**	**1.113**	**−0.4885**

Table A.1
Optimized material streams of the optimized case 4.

No	T (°C)	P (kPa)	$\dot{m}$ (kg/h)	h (kJ/kg)	s (kJ/kg-K)	e (kJ/kg)
LNG1	−159.60	4400.00	100 000.00	−5605.50	4.75	1074.18
LNG2	−61.06	4395.00	100 000.00	−4999.84	8.35	607.47
LNG3	5.69	4390.00	100 000.00	−4812.72	9.12	564.33
F1	−72.57	194.70	127 304.27	−3353.14	2.99	293.28
F2	−71.64	1510.00	127 304.27	−3349.87	3.00	295.03
F3	−5.00	1505.00	127 304.27	−2866.04	4.92	206.23
F4	−5.01	1500.00	127 304.27	−2863.42	4.93	205.76
F5	12.72	1495.00	127 304.27	−2787.87	5.21	198.49
F6	−59.05	199.70	127 304.27	−2877.41	5.31	77.69
HF1	4.74	405.00	52 501.79	−2409.73	3.27	76.33
HF2	1.00	400.00	52 501.79	−2416.08	3.25	76.20
HF3	1.00	400.00	31 499.78	−2414.28	3.25	76.16
HF4	6.50	400.00	21 002.01	−2408.92	3.29	75.49
HF5	3.21	400.00	52 501.79	−2412.14	3.26	75.87
HF6	3.01	390.00	52 501.79	−2412.14	3.27	74.57
H1	1.00	400.00	391 849.19	−15 483.63	2.07	3.87
H2	1.00	400.00	166 744.17	−14 650.51	3.10	2.27
SW1	30.00	101.33	370 842.02	−15 928.40	2.27	0.18
SW2	30.02	415.00	370 842.02	−15 927.99	2.27	0.57
SW3	30.02	415.00	270 343.83	−15 927.99	2.27	0.57
SW4	30.02	415.00	100 498.19	−15 927.99	2.27	0.57
SW5	18.06	410.00	270 343.83	−15 981.36	2.09	0.74
SW6	18.09	410.00	100 498.19	−15 981.21	2.09	0.74
SW7	18.07	410.00	370 842.02	−15 981.32	2.09	0.74
SW8	12.27	405.00	370 842.02	−16 007.26	2.00	1.62
SW9	1.00	400.00	370 842.02	−16 057.72	1.83	4.94
SW10	30.00	101.33	972 597.80	−15 928.40	2.27	0.18
SW11	30.01	200.00	972 597.80	−15 928.27	2.27	0.31
SW12	15.00	195.00	972 597.80	−15 995.25	2.05	0.88
C1	−3.00	140.00	2 589 097.93	−11 993.44	0.22	4.84
C2	−2.99	150.00	2 589 097.93	−11 993.43	0.22	4.86
C3	−10.00	145.00	2 589 097.93	−12 017.22	0.13	7.66
PW1	6.50	400.00	145 743.96	−15 967.38	2.70	2.94
PW2	15.00	395.00	145 743.96	−15 930.68	2.83	1.09
B1	1.00	400.00	225 105.02	−16 100.76	1.30	5.05
B2	15.00	395.00	225 105.02	−16 036.66	1.53	1.15

process achieved zero specific energy consumption of fresh water production and generated extra power for selling. The negative operation and maintenance cost indicated that the process was profitable when producing fresh water. Moreover, the fixed capital investment of the ColdEn-HyDesal(CP)-ORC process was 15.91 million, which was 10.03% higher than that of the ColdEn-HyDesal(C_3H_8)-ORC process. The reason was that the capital cost of the expander in the ColdEn-HyDesal(CP)-ORC process was significantly higher due to the larger power output.

The levelized cost of water of the ColdEn-HyDesal and ColdEn-HyDesal-ORC process were illustrated in Fig. 9. It can be found out that the levelized cost of water of the ColdEn-HyDesal(C_3H_8) process was 2.906 $/m^3. However, the levelized cost of water of the ColdEn-HyDesal(C_3H_8)-ORC process decreased to 2.188 $/m^3 with 24.71% of reduction. These results indicated that integrating ORC into the ColdEn-HyDesal process could reduce the levelized cost of water with the expanse of higher fixed capital investment. The levelized cost of water of the ColdEn-HyDesal(CP) process was 2.471 $/m^3 which was 15.12% lower than the ColdEn-HyDesal(C_3H_8) process. Moreover, the levelized cost of water of the ColdEn-HyDesal(CP)-ORC process was 1.946 $/m^3 with 21.05% decrement compared to the ColdEn-HyDesal(CP) process, which was also 12.16% lower than that of the ColdEn-HyDesal(C_3H_8)-ORC process. This indicated that the ColdEn-HyDesal(CP)-ORC process had the best economic performance.

Table A.2
Optimized material streams of the optimized case 8.

No	T (°C)	P (kPa)	$\dot{m}$ (kg/h)	h (kJ/kg)	s (kJ/kg-K)	e (kJ/kg)
LNG1	−159.60	4400.00	100 000.00	−5605.50	4.75	1074.18
LNG2	−74.14	4395.00	100 000.00	−5051.11	8.10	630.71
LNG3	14.50	4390.00	100 000.00	−4790.30	9.20	563.14
F1	−83.11	123.00	116 389.59	−3403.78	2.96	314.55
F2	−82.00	1765.00	116 389.59	−3399.72	2.97	316.57
F3	−2.01	1760.00	116 389.59	−2871.84	5.07	217.47
F4	−1.69	1755.00	116 389.59	−2860.96	5.11	216.23
F5	14.90	1750.00	116 389.59	−2814.33	5.28	212.59
F6	−72.12	128.00	116 389.59	−2927.49	5.42	57.29
HF1	12.39	106.33	94 666.48	−1524.24	−3.09	0.46
HF2	4.00	101.33	94 666.48	−1537.62	−3.14	1.25
HF3	4.00	101.33	56 799.49	−1537.52	−3.14	1.25
HF4	10.00	101.33	37 866.99	−1528.23	−3.11	0.64
HF5	6.42	101.33	94 666.48	−1533.80	−3.13	0.98
HF6	6.42	101.33	94 666.48	−1533.80	−3.13	0.45
H1	12.39	96.33	94 666.48	−1524.26	−3.09	2.55
H2	4.00	101.33	514 620.22	−13 495.29	0.93	2.71
H3	4.00	101.33	457 820.72	−14 978.83	1.43	1.65
SW1	4.00	101.33	203 208.80	−13 589.77	1.54	0.18
SW2	30.00	101.33	419 953.73	−15 928.40	2.27	0.21
SW3	30.00	121.33	419 953.73	−15 928.37	2.27	0.17
SW4	29.52	116.33	419 953.73	−15 930.52	2.27	0.17
SW5	20.23	111.33	86 090.52	−15 930.52	2.27	0.18
SW6	29.52	116.33	333 863.22	−15 930.52	2.27	0.17
SW7	20.92	111.33	333 863.22	−15 968.92	2.14	0.14
SW8	20.77	111.33	419 953.73	−15 969.55	2.14	0.15
SW9	17.88	106.33	419 953.73	−15 982.47	2.09	0.39
SW10	4.00	101.33	419 953.73	−16 044.57	1.87	3.47
SW11	30.00	101.33	986 371.88	−15 928.40	2.27	0.18
SW12	30.01	200.00	986 371.88	−15 928.27	2.27	0.31
SW13	15.00	195.00	986 371.88	−15 995.25	2.05	0.88
C1	0.00	140.00	2 578 817.40	−11 983.22	0.26	3.85
C2	0.00	150.00	2 578 817.40	−11 983.21	0.26	3.86
C3	−7.00	145.00	2 578 817.40	−12 007.04	0.17	6.37
PW1	10.00	101.33	203 208.80	−13 264.65	1.67	1.49
PW2	10.00	101.33	165 341.82	−15 952.55	2.76	1.68
PW3	15.00	101.33	165 341.82	−15 930.96	2.83	0.74
B1	4.00	101.33	254 611.92	−16 087.45	1.35	3.55
B2	15.00	101.33	254 611.92	−16 037.10	1.52	0.78

5. Conclusions

In this work, a sustainable process (ColdEn-HyDesal-ORC) that integrated organic Rankine cycle (ORC) with hydrate-based desalination (HyDesal) by utilizing LNG cold exergy was proposed and designed to nexus power and water. Different heat transfer performance between the working fluids and the heat sink and heat source were analyzed to reveal the relationship between the exergy destruction and overall performance. Furthermore, the economic comparison between the ColdEn-HyDesal and the ColdEn-HyDesal-ORC was conducted. The main conclusions that were obtained as follows:

1. The ColdEn-HyDesal-ORC process could achieve zero specific energy consumption for desalination and generate extra power.
2. The optimal solution for the ColdEn-HyDesal(CP)-ORC process was achieved by the mixed working fluid comprising 0.9011 of ethane and 0.09899 of propane in the ORC. The net output power and fresh water production of the optimized case 8 was 3480 kW and 165.3 tonne/h, respectively.
3. The non-constant evaporation and condensation temperatures of the mixed working fluid in ORC matched the heat transfer curves of the heat source (seawater) and heat sink (LNG) better than the single working fluid.
4. The lowest total exergy destruction of HEX-6 and HEX-7 was 5518 kW, which was achieved by the optimized case 8 due to the best cold and hot composite curves match by adopting optimal mixed working fluid in ORC.
5. The LNG cold exergy utilization efficiency of the optimized case 2 and 8 was 60.38% and 61.11%, which was 44.87% and 47.67% higher than base cases, respectively. It indicated that the proposed ColdEn-HyDesal-ORC process was highly thermodynamic efficient.
6. The lowest levelized cost of water of the ColdEn-HyDesal-ORC process was 1.946 $\$/m^3$ by adopting CP as hydrate former and ethane/propane mixture as working fluid, which was 21.05% lower than that of the ColdEn-HyDesal process. The results showed that the economic performance of the proposed process was superior to the ColdEn-HyDesal process.

CRediT authorship contribution statement

Tianbiao He: Software, Methodology, Writing - original draft, Funding acquisition. **Jibao Zhang:** Visualization, Data curation. **Ning Mao:** Validation, Investigation. **Praveen Linga:** Conceptualization, Writing - review & editing.

Declaration of competing interest

The authors declare that they have no known competing financial interests or personal relationships that could have appeared to influence the work reported in this paper.

Acknowledgments

The authors would like to appreciate the funding support of the National Natural Science Foundation of China (No. 51906225), the Shandong Provincial Natural Science Foundation, China (No. ZR2019QEE020), and the Fundamental Research Funds for the Central Universities, China (No. 19CX02011A).

Appendix A

See Tables A.1 and A.2.

Appendix B. Supplementary data

Supplementary material related to this article can be found online at https://doi.org/10.1016/j.apenergy.2021.116839.

References

[1] China Statistical Bureau. China statistical yearbook. China Stat Publ House 2019;9:3.
[2] Lin Wensheng, Zhang Na, Gu Anzhong. LNG (liquefied natural gas): A necessary part in China's future energy infrastructure. Energy 2010;35(11):4383–91.
[3] He Tianbiao, Chong Zheng Rong, Zheng Junjie, Ju Yonglin, Linga Praveen. LNG cold energy utilization: Prospects and challenges. Energy 2019;170:557–68.
[4] He Tianbiao, Liu Zuming, Ju Yonglin, Parvez Ashak Mahmud. A comprehensive optimization and comparison of modified single mixed refrigerant and parallel nitrogen expansion liquefaction process for small-scale mobile LNG plant. Energy 2019;167:1–12.
[5] Kanbur Baris Burak, Xiang Liming, Dubey Swapnil, Choo Fook Hoong, Duan Fei. Cold utilization systems of LNG: A review. Renew Sustain Energy Rev 2017;79:1171–88.
[6] IGU world LNG report 2020. Technical report, International Gas Union; 2020.
[7] Xie Xiaorong, Liu Ping, Bai Kai, Han Yingduo. Applying improved blocking filters to the SSR problem of the Tuoketuo power system. IEEE Trans Power Syst 2012;28(1):227–35.
[8] He Tianbiao, Mao Ning, Liu Zuming, Qyyum Muhammad Abdul, Lee Moonyong, Pravez Ashak Mahmud. Impact of mixed refrigerant selection on energy and exergy performance of natural gas liquefaction processes. Energy 2020;199:117378.
[9] Cao Wensheng, Beggs Clive, Mujtaba Iqbal M. Theoretical approach of freeze seawater desalination on flake ice maker utilizing LNG cold energy. Desalination 2015;355:22–32.
[10] Xia Wenkai, Huo Yaowu, Song Yunfei, Han Jianming, Dai Yiping. Off-design analysis of a CO2 Rankine cycle for the recovery of LNG cold energy with ambient air as heat source. Energy Convers Manage 2019;183:116–25.
[11] Mehrpooya Mehdi, Esfilar Reza, Moosavian SM Ali. Introducing a novel air separation process based on cold energy recovery of LNG integrated with coal gasification, transcritical carbon dioxide power cycle and cryogenic CO2 capture. J Cleaner Prod 2017;142:1749–64.
[12] Zhao Liang, Dong Hui, Tang Jiajun, Cai Jiuju. Cold energy utilization of liquefied natural gas for capturing carbon dioxide in the flue gas from the magnesite processing industry. Energy 2016;105:45–56.
[13] Zhang Guoqiang, Zheng Jiongzhi, Yang Yongping, Liu Wenyi. A novel LNG cryogenic energy utilization method for inlet air cooling to improve the performance of combined cycle. Appl Energy 2016;179:638–49.
[14] Liu Zuming, Karimi Iftekhar A, He Tianbiao. A novel inlet air cooling system based on liquefied natural gas cold energy utilization for improving power plant performance. Energy Convers Manage 2019;187:41–52.
[15] Zhang Na, Lior Noam. A novel near-zero CO2 emission thermal cycle with LNG cryogenic exergy utilization. Energy 2006;31(10–11):1666–79.
[16] Shi Xiaojun, Che Defu. A combined power cycle utilizing low-temperature waste heat and lng cold energy. Energy Convers Manage 2009;50(3):567–75.
[17] Querol E, Gonzalez-Regueral B, García-Torrent J, Ramos Alberto. Available power generation cycles to be coupled with the liquid natural gas (LNG) vaporization process in a Spanish LNG terminal. Appl Energy 2011;88(7):2382–90.
[18] Lee Ung, Park Keonhee, Jeong Yeong Su, Lee Sangho, Han Chonghun. Design and analysis of a combined rankine cycle for waste heat recovery of a coal power plant using LNG Cryogenic Exergy. Ind Eng Chem Res 2014;53(23):9812–24.
[19] García Ramón Ferreiro, Carril Jose Carbia, Gomez Javier Romero, Gomez Manuel Romero. Combined cascaded rankine and direct expander based power units using LNG (liquefied natural gas) cold as heat sink in LNG regasification. Energy 2016;105:16–24.
[20] Ghaebi Hadi, Parikhani Towhid, Rostamzadeh Hadi. Energy, exergy and thermoeconomic analysis of a novel combined cooling and power system using low-temperature heat source and LNG cold energy recovery. Energy Convers Manage 2017;150:678–92.
[21] Bao Junjiang, Zhang Ruixiang, Lin Yan, Zhang Ning, Zhang Xiaopeng, He Gaohong. The effect of the arrangements for compression process and expansion process on the performance of the two-stage condensation Rankine cycle. Energy Convers Manage 2018;159:299–311.
[22] Sun Qingxuan, Wang Yaxiong, Cheng Ziyang, Wang Jiangfeng, Zhao Pan, Dai Yiping. Thermodynamic and economic optimization of a double-pressure organic Rankine cycle driven by low-temperature heat source. Renew Energy 2020;147:2822–32.
[23] Sun Zhixin, Zhang Han, Zhang Tianfeng, Lin Li, Lin Kui. Optimizations and comparison of three two-stage Rankine cycles under different heat source temperatures and NG distribution pressures. Energy Convers Manage 2020;209:112655.
[24] Babu Ponnivalavan, Nambiar Abhishek, He Tianbiao, Karimi Iftekhar A, Lee Ju Dong, Englezos Peter, et al. A review of clathrate hydrate based desalination to strengthen Energy–Water nexus. ACS Sustain Chem Eng 2018;6(7):8093–107.
[25] Cai Lichao, Pethica Brian A, Debenedetti Pablo G, Sundaresan Sankaran. Formation of cyclopentane methane binary clathrate hydrate in brine solutions. Chem Eng Sci 2016;141:125–32.
[26] Babu Ponnivalavan, Kumar Rajnish, Linga Praveen. Unusual behavior of propane as a co-guest during hydrate formation in silica sand: Potential application to seawater desalination and carbon dioxide capture. Chem Eng Sci 2014;117:342–51.
[27] Ho-Van Son, Bouillot Baptiste, Douzet Jérome, Babakhani S Maghsoodloo, Herri Jean-Michel. Cyclopentane hydrates–A candidate for desalination?. J Environ Chem Eng 2019;7(5):103359.
[28] Zheng Jia-nan, Yang Mingjun. Experimental investigation on novel desalination system via gas hydrate. Desalination 2020;478:114284.
[29] Khan Muhammad Naveed, Peters Cor J, Koh Carolyn A. Desalination using gas hydrates: The role of crystal nucleation, growth and separation. Desalination 2019;468:114049.
[30] He Tianbiao, Nair Sajitha K, Babu Ponnivalavan, Linga Praveen, Karimi Iftekhar A. A novel conceptual design of hydrate based desalination (HyDesal) process by utilizing LNG cold energy. Appl Energy 2018;222:13–24.
[31] He Tianbiao, Chong Zheng Rong, Babu Ponnivalavan, Linga Praveen. Techno-economic evaluation of cyclopentane hydrate-based desalination with liquefied natural gas cold energy utilization. Energy Technol 2020;8(8):1900212.
[32] Chong Zheng Rong, He Tianbiao, Babu Ponnivalavan, Zheng Jia-nan, Linga Praveen. Economic evaluation of energy efficient hydrate based desalination utilizing cold energy from liquefied natural gas (LNG). Desalination 2019;463:69–80.
[33] Aspen HYSYS V100. 2017, https://www.aspentech.com/.
[34] Peng Ding-Yu, Robinson Donald B. A new two-constant equation of state. Ind Eng Chem Fundam 1976;15(1):59–64.
[35] Yu Haoshui, Kim Donghoi, Gundersen Truls. A study of working fluids for Organic Rankine Cycles (ORCs) operating across and below ambient temperature to utilize liquefied natural gas (LNG) cold energy. Energy 2019;167:730–9.
[36] Yu Haoshui, Gundersen Truls, Gençer Emre. Optimal liquified natural gas (LNG) cold energy utilization in an Allam cycle power plant with carbon capture and storage. Energy Convers Manage 2021;228:113725.
[37] Hassan Rania, Cohanim Babak, De Weck Olivier, Venter Gerhard. A comparison of particle swarm optimization and the genetic algorithm. In: 46th AIAA/ASME/ASCE/AHS/ASC structures, structural dynamics and materials conference. 2005, p. 1897.
[38] Duan Yao, Harley RG, Habetler TG. Comparison of particle swarm optimization and genetic algorithm in the design of permanent magnet motors. In: 2009 IEEE 6th international power electronics and motion control conference. IEEE; 2009, p. 822–5.
[39] Khan Mohd Shariq, Ali Wahid, Qyyum Muhammad Abdul, Ansari Khursheed B, Lee Moonyong. Introduction to particle swarm optimization and its paradigms: A bibliographic survey. In: AI and machine learning paradigms for health monitoring system: Intelligent data analytics. p. 105.
[40] MathWorks. 2018, https://www.mathworks.com/.
[41] He Tianbiao, Lv Hongyu, Shao Zixian, Zhang Jibao, Xing Xialian, Ma Huigang. Cascade utilization of LNG cold energy by integrating cryogenic energy storage, organic Rankine cycle and direct cooling. Appl Energy 2020;277:115570.
[42] Moran Michael J, Shapiro Howard N, Boettner Daisie D, Bailey Margaret B. Fundamentals of engineering thermodynamics. John Wiley & Sons; 2014.
[43] Caldera Upeksha, Breyer Christian. Learning curve for seawater reverse osmosis desalination plants: Capital cost trend of the past, present, and future. Water Resour Res 2017;53(12):10523–38.
[44] Wakui Tetsuya, Kawayoshi Hiroki, Yokoyama Ryohei. Optimal structural design of residential power and heat supply devices in consideration of operational and capital recovery constraints. Appl Energy 2016;163:118–33.
[45] Rovira Antonio, Barbero Rubén, Montes María José, Abbas Rubén, Varela Fernando. Analysis and comparison of integrated solar combined cycles using parabolic troughs and linear fresnel reflectors as concentrating systems. Appl Energy 2016;162:990–1000.
[46] Bejan Adrian, Tsatsaronis George. Thermal design and optimization. John Wiley & Sons; 1996.